Research Article Vol. 31, No. 4 / 13 Feb 2023 / Optics Express 5872
Optics EXPRESS

Development and characterization of PILOT: a transportable instrument for laser-induced grating spectroscopy

PRIYAV SHAH,* LAURENT M. LE PAGE, AND BENJAMIN A. O. WILLIAMS

Department of Engineering Science, University of Oxford, Oxford, UK
priyav.shah@eng.ox.ac.uk

Abstract: Laser-induced grating spectroscopy (LIGS) is an optical diagnostic technique for gas-phase thermometry in challenging environments where physical probes are undesirable. The Portable In-line LIGS for Optical Thermometry (PILOT) instrument is a novel self-contained, compact device capable of tracer-free LIGS measurements at 400 Hz. It can be mounted in any orientation and includes internal alignment capability, adjustable path length matching for the pump beams, and an energy/power attenuation mechanism for the pump/probe beams. Characterization of the instrument demonstrated that it can produce accurate (<0.37% in ambient air) and precise (±0.7% in ambient air) spatially- and temporally-resolved temperature measurements, and is now ready to be deployed in research facilities.

1. Introduction

Laser-Induced Grating Spectroscopy (LIGS) is a multiparameter four-wave mixing diagnostic. Although primarily used to obtain point temperature [1] measurements in gases, LIGS has also been employed for pressure measurements [2], species detection [3] and velocimetry [4]. Recent developments of the technique include a new, simpler approach to measure the pressure of a gas [5] as well as the simultaneous measurements of temperature and species concentration in a flame [6]. The use of the technique at 100 kHz [7] using a pulse burst laser has been demonstrated, as has the potential for LIGS using a femtosecond laser [8]. Furthermore, LIGS has been extended for 1-D temperature measurements [9]. These developments have led to an increased interest in the technique, leading to its deployment in applications ranging from flame thermometry [10] and engine research [11] to wind tunnels [12].

The LIGS technique has two variants: Laser-Induced Thermal Grating Spectroscopy (LITGS) and Laser-Induced Electrostrictive Grating Spectroscopy (LIEGS). The optical setup for both is identical; two pulsed laser beams (known as the 'pump' beams) are crossed over at the measurement point to create a periodic fringe pattern (the fringe spacing is determined by the crossing angle). In the case of LITGS, resonant absorption of the pump laser energy by gas molecules, followed by rapid collisional quenching of these molecules, leads to the formation of a temporally evolving volumetric density perturbation. There is a stationary, spatially-periodic density perturbation component due to localized temperature variation, as well as a time-varying component formed by counter-propagating acoustic waves (which interact to produce a standing wave) created by the sudden deposition of energy into the fluid. For LIEGS, a spatially periodic deformation is applied to the gas through the electrostrictive process; the sudden creation of a density perturbation again results in the formation of counter-propagating acoustic waves and a subsequent standing wave. Therefore both LITGS and LIEGS, through resonant absoprtion and electrostriction, respectively, result in a spatial density modulation which induces a spatial

#482477 https://doi.org/10.1364/OE.482477
Journal © 2023 Received 6 Dec 2022; revised 19 Jan 2023; accepted 21 Jan 2023; published 2 Feb 2023

Optics EXPRESS

modulation in the refractive index of the gas (called a grating). The strength of the grating varies ('beats') in time at a frequency determined by the local speed of sound. A continuous wave 'probe' beam can be directed at the grating at the first-order Bragg-angle such that the efficiency with which the probe beam is scattered by the grating varies with the beat frequency of the grating. This scattered 'signal' beam is collected by a detector, and the frequency of the recorded oscillations (F) is related to the temperature (T) for ideal gases by the equation

$$T = \frac{\Lambda^2 M F^2}{\gamma k_B} \tag{1}$$

where Λ is the fringe spacing, M is the molecular mass of the gas, γ is the heat capacity ratio for the gas, and k_B is Boltzmann's constant. Although LIEGS does not require a resonant species to be present and is therefore inherently tracer-free, the strength of a LITGS signal can be orders of magnitude larger than a LIEGS signal created using the same optical setup. Furthermore, LITGS can still be 'tracer-free' in the case that a resonant species is naturally present in the system. Both variants are therefore useful depending on the application.

LIGS is particularly attractive as an optical diagnostic technique because its coherent laser-like signal beam can enable background discrimination leading to an excellent signal-to-noise ratio, enabling its application in challenging environments. Compared to similar techniques such as Coherent Anti-Stokes Raman Scattering (CARS), LIGS features a significantly simpler and cheaper experimental setup [6]. In order to capitalize on this notable advantage and increase the accessibility of the technique, a compact transportable instrument has been designed, manufactured, and characterized. While the use of a compact setup has been reported before [13], it was only capable of measurements at 10 Hz, required a cumbersome external optical setup for alignment, and was designed primarily for LITGS measurements (which necessitated the use of a tracer species for many applications). The Portable In-line LIGS for Optical Thermometry (PILOT) instrument is an entirely self-contained device capable of both LITGS and tracer-free LIEGS measurements at 400 Hz.

2. Design of PILOT instrument

The instrument consists of the PILOT device which contains the laser heads and optics, a supporting trolley ('co-PILOT') on which the laser power supplies are mounted, and a 'detection rail' which holds the optics required to collect the signal.

2.1. PILOT device

The PILOT device consists of a breadboard on which the laser heads and optics are mounted, and an enclosure around it. To minimize the device footprint, the laser heads are secured underneath the breadboard while the optics are on top. A diode-pumped Nd:YAG laser (Quantel Merion C) emitting light at a wavelength of 1064 nm with a pulse energy of 100 mJ and a repetition rate of up to 400 Hz is used to deliver the pump beams. A GLR-20 fiber laser from IPG Photonics is used to produce a continuous wave probe beam at a wavelength of 532 nm and power of up to 20 W. Periscopes are utilized to direct the beams to the top of the breadboard. From there, the probe beam passes through an adjustable mirror and fixed prism before arriving at a crossing lens. The beam from the pulsed laser passes through an adjustable attenuator before being split into the two pump beams by a 50:50 beam splitter. Both pump beams are subsequently directed onto the crossing lens by mirrors. The path of one of the beams includes a 'delay line', achieved by placing two mirrors on a translation stage, to allow for the path lengths of both pump beams to be matched. A Thorlabs collimated DPSS laser module (model CPS-532C2) is also fixed on the top of the breadboard, and used to create a 'signal tracing beam' which mimics the path of the signal beam allowing accurate placement of the detection optics. The crossing lens focuses and crosses

Optics EXPRESS

all four beams. The default configuration for the device is to use a 750 mm focal length crossing lens which results in a crossing angle of 3° for the pump beams. Different geometries can be used by installing a crossing lens with a different focal length. To meet safety specifications, a lens tube encloses all the beams as they exit the device. The layout is shown in Fig. 1.

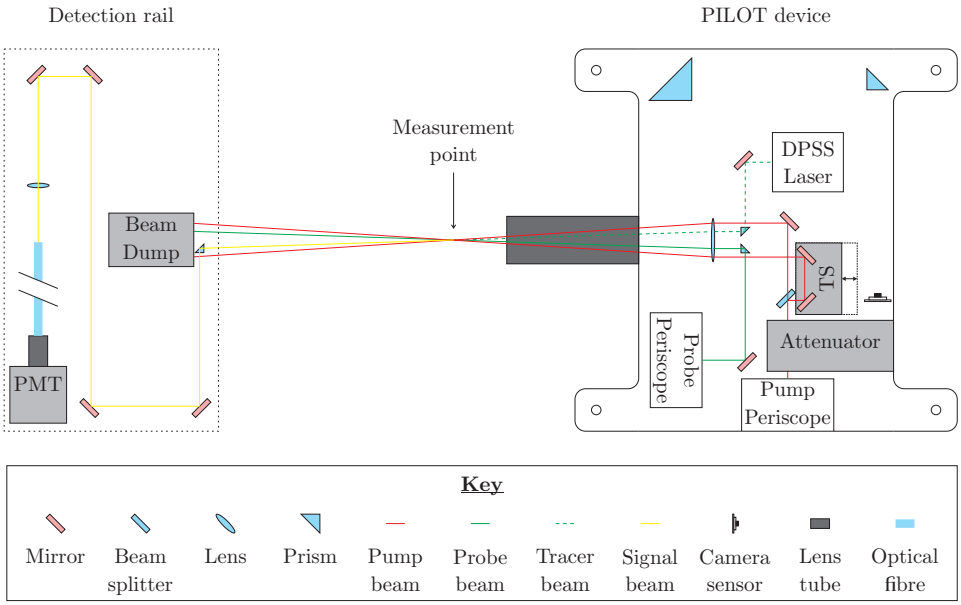

Fig. 1. Schematic of the top deck of the PILOT system (showing the path of the pump, probe and signal tracing beams) and the detection rail optics (showing the termination of the pump and probe beams, and the path of the signal beam). Note that the tracer beam is only used to position the detection rail (and is turned off during operation). TS indicates the translation stage.

For this default geometry, the pump beams were measured (using a Thorlabs BC106N CCD Camera Beam Profiler) to be 342 µm wide at the crossing point. This results in an overlap region that is 12.8 mm long and has a maximum height and width of 342 µm, respectively. After accounting for the rhomboidal shape of the grating, the effective spatial resolution is anticipated to be 6 mm x 0.3 mm x 0.3 mm [13].

In addition to LIEGS measurements, the PILOT instrument also collects LITGS measurements when a species that resonantly absorbs 1064 nm is present. This has been shown to be advantageous in applications such as combustion, where naturally-occurring water permits the acquisition of tracer-free LITGS signals [6] in the end gas (that cannot be seeded with a tracer). Furthermore, the capability to simultaneously obtain LIEGS and LITGS signals has been shown to enable the concentration of resonant species to be measured by considering the ratio between the intensities of the LIEGS and LITGS signals [14].

2.2. Signal detection

A Thorlabs optical rail is used to carry the optics required for signal detection. This includes a beam dump to terminate the pump and probe beams and a series of mirrors and prisms to direct the signal beam along the optical rail multiple times. This ensures a long optical path which helps discriminate the signal beam from any incoherent scattered light (e.g., from windows placed near the measurement point). Finally, a lens is used to focus the beam into an optical fiber which leads to a detector. The detector used is a H10721-20 photomultiplier tube (PMT) module

Optics EXPRESS

from Hamamatsu. The full optical layout is shown in Fig. 1. Depending on the application, other optics (such as a spatial filter) can be added to the rail to process the signal beam. The signal from the PMT is digitized by an oscilloscope (Picoscope 6424E by Pico Technology).

2.3. Internal alignment

The PILOT device incorporates an internal alignment mechanism which enables quick and easy alignment on-site without the need for an extensive optical reconfiguration. To perform this, a prism on a magnetic mount is installed after the crossing lens. This prism reflects the pump, probe and signal tracing beams successively onto two other prisms, and finally onto a CCD sensor (Raspberry Pi NoIR Camera V2 module). The distance between the camera and the crossing lens is equal to the focal length of the lens, so the camera is used to ensure that all four beams are overlapped at the crossing point. To ensure the safe termination of any laser beams exiting the PILOT device during alignment, the external lens tube is removed and a beam dump is secured onto the output face. This layout is depicted in Fig. 2.

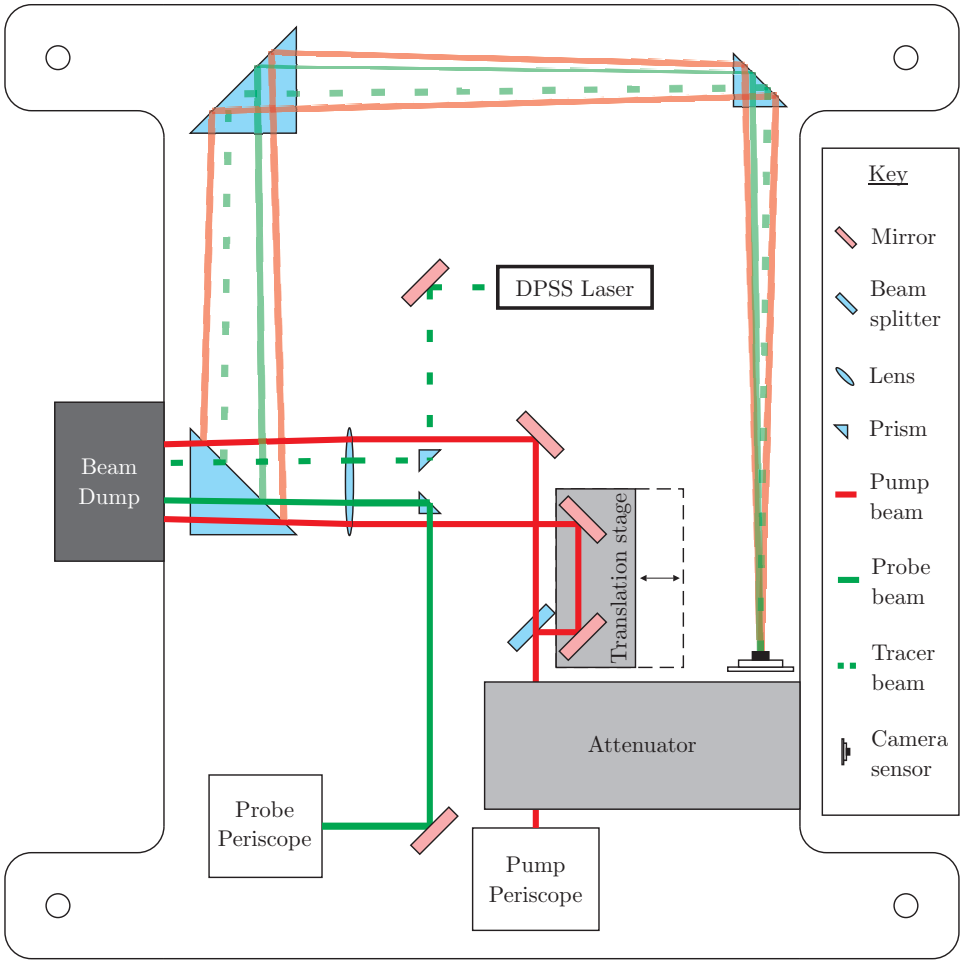

Fig. 2. Schematic of the top deck of the PILOT system, showing the path of the pump, probe and signal tracing beams during internal alignment. The external lens tube has been replaced with a beam dump.

Optics EXPRESS

2.4. Mechanical considerations and peripherals

A Raspberry Pi computer interfaces with the CCD sensor for beam alignment. It is located underneath the breadboard within the PILOT device, alongside the pump and probe lasers, and accessed remotely to enhance portability and ensure compactness. This integration also allows it to be used as the power source for the Thorlabs DPSS laser module.

Protrusions from the four corners of the PILOT device, including mounting holes, enable the PILOT device to be installed onto a frame in any orientation. The entire device is enclosed to meet laser safety requirements, and the lid can be opened to provide easy access to any optical components that may require adjustment during alignment. The dimensions of the device are 460 mm x 310 mm x 280 mm, and it weighs ~ 20 kg. Figure 3 depicts the enclosed device.

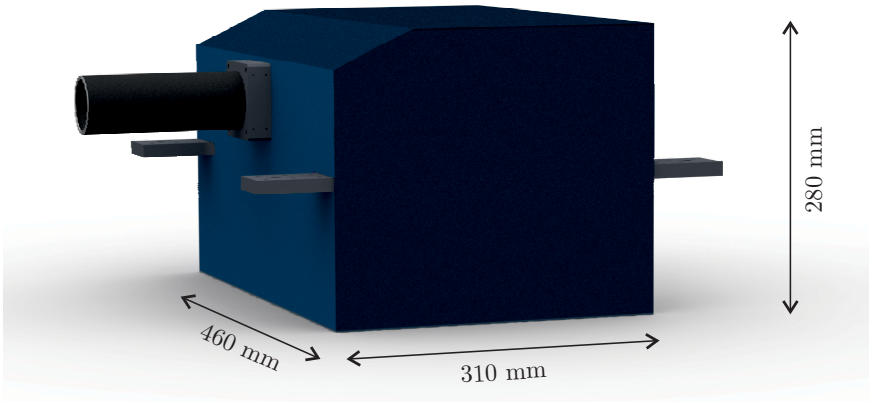

Fig. 3. Rendered image of the PILOT device. Note the grey protrusions which allow for the device to be mounted.

The laser umbilicals connecting back to 'Co-PILOT' are 3 m long. Co-PILOT has wheels and mechanically-lowered feet which enable it to be easily maneuvered into place and stabilized during operation. The PILOT device can be secured on top of co-PILOT during transportation and/or operation. The detection rail can also be mounted on co-PILOT during transportation.

A standard electrical socket and laser interlock system are the only external requirements for the instrument. Once aligned, the entire system can be run remotely which allows for deployment in potentially dangerous environments.

3. Characterization of PILOT

Following the design and manufacture of the PILOT instrument, its performance in room air (i.e., tracer-free LIEGS) was characterized.

3.1. Accuracy and precision

To determine the accuracy and precision of the PILOT instrument, LIEGS temperature measurements taken at a repetition rate of 400 Hz in ambient air were compared to data logged by two thermocouples placed above and below the LIEGS measurement volume.

Exposed-junction K-type thermocouples with junction diameters of 1 mm and 0.65 mm, respectively, were used. Data acquired from the thermocouples were logged using a DrDAQ data logger by Pico Technology, while LIEGS signals were recorded using a Wavesurfer 3074 oscilloscope from Teledyne LeCroy (the Picoscope 6424E, as described in Section 2.2 and used for all other experiments, was unavailable for this test). A pulse generator (model TGP110 from

Optics EXPRESS

Aim & Thurlby Thandar Instruments) was employed to provide a synchronising pulse to the data logger and oscilloscope. The data were collected for 1 second at 400 Hz.

Figure 4 shows a normalized LIEGS signal, consisting of 2002 data points, recorded during the experiment. To extract the oscillation frequency from the signals, a Fast Fourier Transform (FFT) routine was used. First, the signals were zero-padded to a length of 2^{16} points to increase the final resolution of the signal in the frequency domain. A FFT was applied to the signals, and the peak frequency from the resulting power spectrum was determined. This frequency was then substituted into Eq. (1), together with the relevant thermodynamic properties of air and the fringe spacing created by the PILOT instrument, to obtain the measured temperature.

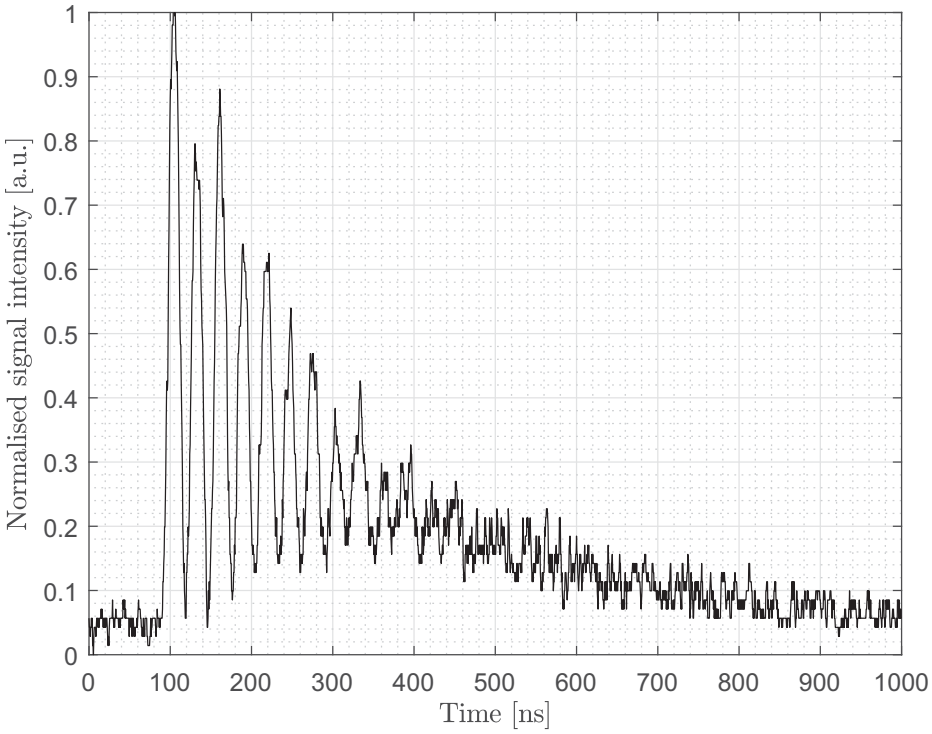

Fig. 4. Normalized single-shot LIGS signal obtained from ambient air.

Table 1 displays the mean temperatures measured by each measurement device/technique. The uncertainty in the thermocouple measurements (±1 K) is the stated error of the amplifiers that were used (AD8495 K-type thermocouple amplifiers from Analog Devices). The stated uncertainty in the LIEGS measurement is the standard deviation from the mean for the dataset.

Table 1. Steady-state thermocouple and LIEGS temperature measurements at room temperature and pressure.

Thermocouple 1 [K]	Thermocouple 2 [K]	LIEGS [K]
297.5 ±1	299.5 ±1	298.6 ±2.2

The data show that temperature measurements taken by the PILOT instrument in ambient air lie within the stated accuracy of the two K-type thermocouples used for this experiment. This indicates a PILOT temperature measurement accuracy of better than 0.37%. The single shot precision of the PILOT instrument in ambient air is ±0.7%.

Optics EXPRESS

3.2. Delay line

A delay line was included in one of the pump beam paths to allow for path length matching between both pump beams. The effect of retarding the phase of one beam relative to the other was investigated. For this experiment, the translation stage in the delay line was moved in steps of 1 mm (which equates to a 2 mm change in the path length of the relevant pump beam). At each position, 100 signals were collected (in ambient room air). The pump beams were set to full energy (100 mJ from the pulsed laser), but the probe beam was attenuated to 2 W to ensure that the signal strength remained within the linear regime of the PMT.

Figure 5 shows the mean LIGS signal intensity achieved at each position, with the error bars showing 1 standard deviation of the data from the mean. The data show good agreement with a Gaussian fit, which is consistent with the observations by Stampanoni-Panariello *et al.* [15]. The full width at half maximum (FWHM) of the Gaussian fit was 4.4 mm. This behaviour, caused by the coherence length of the pump laser, shows that a misalignment of the position of the mirrors by only ~ 3 mm either side of the optimal position would result in a 50% decrease in signal intensity, highlighting the benefit of this degree of adjustment.

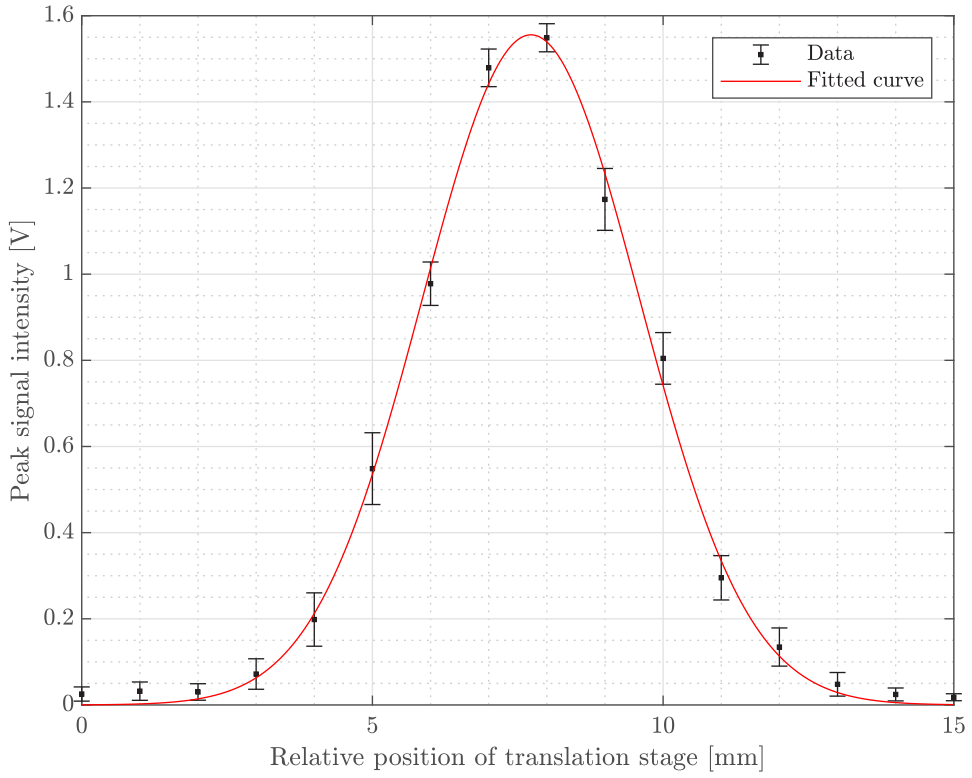

Fig. 5. Variation of LIEGS signal strength as the delay line translation stage is moved. Each point is the mean of 100 data points, and the error bars signify 1 standard deviation from the mean. The red line shows a least-squares Gaussian fit.

Optics EXPRESS

3.3. Energy and power scaling

Certain applications of the PILOT instrument may require the pump beams to be attenuated (e.g., due to window damage thresholds) or the probe beam power to be reduced (e.g., due to excessive stray light). The effect of pump beam pulse energy and probe beam power on signal strength was therefore characterized.

To quantify the effect of the probe beam power, a UP19K-15S-VR-D0 thermopile power meter from Gentec was placed in the path of the probe beam after the grating (so that losses within the PILOT device were accounted for). The device was run at 400 Hz and the probe power was varied between setpoints of 0.5 W and 9 W. In order to remain within the linear regime of the PMT, the probe power was not increased further. Figure 6 shows the mean peak signal intensity for the LIEGS signals collected at different probe powers. The results show a linear trend, which was expected as an increase in probe power results in a proportional increase in the light scattered off the grating to form the signal beam.

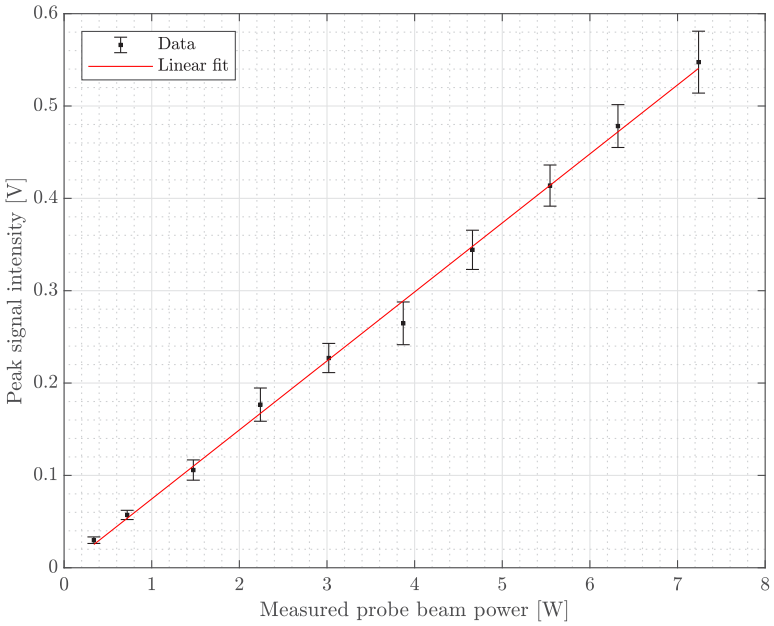

Fig. 6. Variation of LIEGS signal strength as the probe power was increased. Each point is the mean of 400 data points, and the error bars signify 1 standard deviation from the mean. The red line shows a least-squares linear fit.

To measure the variation in pump beam energy, a model S470C thermopile power meter from Thorlabs was placed in the path of one of the pump beams. The probe beam was kept at a constant power, and the attenuator module within the PILOT device was used to increase the pump beam energy. Due to the damage threshold of the power meter, the device was run at 10 Hz and an absorptive neutral density filter (for which the attenuation was calibrated beforehand) had to be placed in front of the meter. Figure 7 shows the mean peak signal intensity for the LIEGS signals collected for varying pump beam energies. A least-squares quadratic fit has been applied to the data, which shows that the signal beam intensity increased as a function of the pump beam energy squared. The R-squared value, which is a measure of the strength of the correlation, was 99.7%. This is in agreement with the theory derived by Stampanoni-Panariello *et al.* [16], who showed that the diffraction efficiency of the grating (which they denote as η) is proportional to the squared pump energy.

Optics EXPRESS

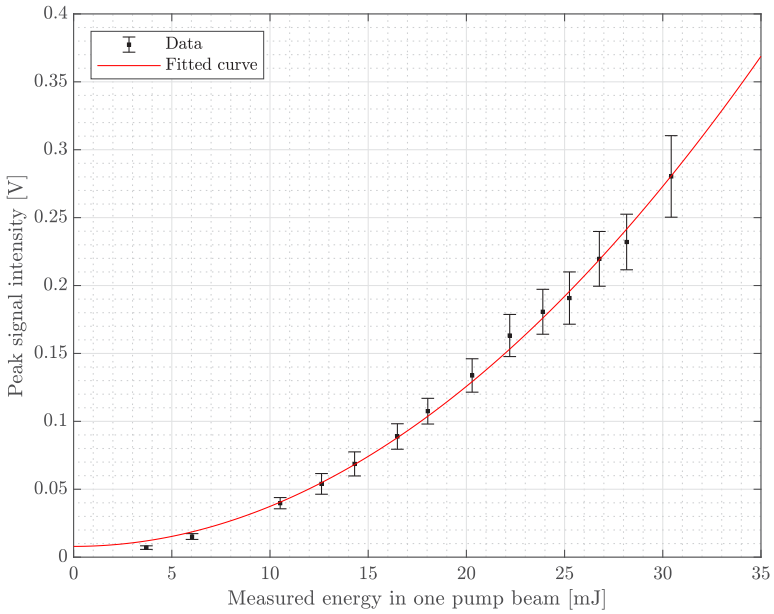

Fig. 7. Variation of mean LIGS signal strength as the pump energy was increased. Each point is the mean of 400 data points, and the error bars signify 1 standard deviation from the mean. The red line shows a least-squares fit.

4. Conclusions

The development and characterization of the Portable In-line Laser-Induced Grating Spectroscopy (LIGS) for Optical Thermometry (PILOT) instrument has been presented. PILOT is a compact, self-contained instrument that incorporates a pulsed laser (emitting 100 mJ pulses at 1064 nm) and a continuous wave laser (emitting up to 20 W at 532 nm). This enables it to conduct both LITGS and tracer-free LIEGS measurements at up to 400 Hz, unlocking applications that would have been impossible in the past. For flexibility and ease-of-use, the device can be mounted in any orientation and includes internal alignment capability. PILOT displayed a temperature measurement accuracy of better than 0.37% and a single shot precision of ±0.7% in ambient air.

The design of PILOT includes an adjustable delay line to allow tunablity of temporal phase matching between the two pump beams. The importance of this flexibility was characterized, showing that a misalignment of the delay line by only ~ 3 mm either side of the optimal position would result in a 50% decrease in signal intensity. The device also includes the capability of attenuating the pump beam energies and/or the probe beam power. The effect of both was investigated, and it was found that the signal intensity scaled linearly with probe power but quadratically with pump energy (with air as the test gas).

With the baseline performance of the PILOT system demonstrated, future work will take advantage of its unique design features to deploy it in a wide range of research facilities including, but not limited to, wind tunnels, shock tubes, and combustors.

Funding. Engineering and Physical Sciences Research Council (EP/N509711/1, EP/P000878/1).

Acknowledgments. P. Shah acknowledges support from an Engineering and Physical Sciences Research Council (EPSRC) studentship.

Disclosures. All authors: Oxford University Innovation (P).

Data availability. Data underlying the results presented in this paper are available in Ref. [17].

Optics EXPRESS

References

1. B. Scott, C. Willman, B. Williams, P. Ewart, R. Stone, and D. Richardson, "In-cylinder temperature measurements using laser induced grating spectroscopy and two-colour plif," SAE Int. J. Engines **10**(4), 2191–2201 (2017).
2. A.-L. Sahlberg, A. Luers, C. Willman, B. Williams, and P. Ewart, "Pressure measurement in combusting and non-combusting gases using laser-induced grating spectroscopy," Appl. Phys. B **125**(3), 46 (2019).
3. M. S. Brown, P. A. DeBarber, E. B. Cummings, and H. G. Hornung, "Trace species concentration and temperature measurements at high pressure using laser-induced grating spectroscopy," in *Optical Techniques in Fluid, Thermal, and Combustion Flow*, vol. 2546 (International Society for Optics and Photonics, 1995), pp. 519–529.
4. S. Schlamp, E. B. Cummings, and T. H. Sobota, "Laser-induced thermal-acoustic velocimetry with heterodyne detection," Opt. Lett. **25**(4), 224–226 (2000).
5. C. Willman, L. M. L. Page, P. Ewart, and B. A. O. Williams, "Pressure measurement in gas flows using laser-induced grating lifetime," Appl. Opt. **60**(15), C131–C141 (2021).
6. F. De Domenico, T. F. Guiberti, S. Hochgreb, W. L. Roberts, and G. Magnotti, "Temperature and water measurements in flames using 1064 nm laser-induced grating spectroscopy (ligs)," Combust. Flame **205**, 336–344 (2019).
7. F. D. Domenico, T. F. Guiberti, S. Hochgreb, W. L. Roberts, and G. Magnotti, "Tracer-free laser-induced grating spectroscopy using a pulse burst laser at 100 khz," Opt. Express **27**(22), 31217–31224 (2019).
8. Y. Wu, M. Zhuzou, T. Zhao, P. Ding, S. Sun, J. Wang, Z. Liu, and B. Hu, "Gas-phase pressure measurement using femtosecond laser-induced grating scattering technique," Opt. Lett. **47**(7), 1859–1862 (2022).
9. C. Willman and P. Ewart, "Multipoint temperature measurements in gas flows using 1-d laser-induced grating scattering," Exp. Fluids **57**(12), 191 (2016).
10. D. Hot, A.-L. Sahlberg, M. Aldén, and Z. Li, "Mid-infrared laser-induced thermal grating spectroscopy of hot water lines for flame thermometry," Proc. Combust. Inst. **38**(1), 1885–1893 (2021).
11. C. Willman, R. Stone, M. Davy, B. Williams, P. Ewart, L. Shen, D. Hung, M. Liu, and J. Camm, "Cycle-to-cycle variation analysis of two-colour plif temperature measurements calibrated with laser induced grating spectroscopy in a firing gdi engine," SAE Int. J. Adv. Curr. Pract. **1**, 722 (2019).
12. C. Selcan, T. Sander, and C. Mundt, "In situ nozzle reservoir thermometry by laser-induced grating spectroscopy in the helm free-piston reflected shock tunnel," Shock. Waves **31**(6), 551–570 (2021).
13. F. Förster, C. Crua, M. Davy, and P. Ewart, "Temperature measurements under diesel engine conditions using laser induced grating spectroscopy," Combust. Flame **199**, 249–257 (2019).
14. T. Seeger, J. Kiefer, M. C. Weikl, A. Leipertz, and D. N. Kozlov, "Time-resolved measurement of the local equivalence ratio in a gaseous propane injection process using laser-induced gratings," Opt. Express **14**(26), 12994–13000 (2006).
15. A. Stampanoni-Panariello, B. Hemmerling, and W. Hubschmid, "Electrostrictive generation of nonresonant gratings in the gas phase by multimode lasers," Phys. Rev. A **51**(1), 655–662 (1995).
16. A. Stampanoni-Panariello, D. Kozlov, P. Radi, and B. Hemmerling, "Gas phase diagnostics by laser-induced gratings i. theory," Appl. Phys. B **81**(1), 101–111 (2005).
17. P. Shah, L. M. Le Page, and B. A. O. Williams, Data for "Development and characterization of PILOT: a transportable instrument for laser-induced grating spectroscopy," University of Oxford (2022), https://doi.org/10.5287/bodleian:2a86V958e.